JOURNAL OF COLLOID AND INTERFACE SCIENCE **184,** 112–122 (1996)
ARTICLE NO. 0601

The Effect of Impeller Type on Floc Size and Structure during Shear-Induced Flocculation

PATRICK T. SPICER, WOLFGANG KELLER, AND SOTIRIS E. PRATSINIS[1]

Department of Chemical Engineering, University of Cincinnati, Cincinnati, Ohio 45221-0171

Received February 9, 1996; accepted June 19, 1996

The effect of impeller type and shear rate on the evolution of floc size and structure during shear-induced flocculation of polystyrene particles with aluminum sulfate is investigated by image analysis. One radial flow (six-blade Rushton turbine) and two axial flow (three-blade fluid foil, four-blade 45° pitch) impeller configurations are examined. The steady state average floc size is shown to depend on the frequency of recirculation to the impeller zone and its characteristic velocity gradient. The concepts of fractal geometry are used to characterize the floc structure. For all impellers, the two-dimensional floc fractal dimension, D_{pf}, increases during floc growth, indicating formation of more open structures. Later on, D_{pf} levels off at a steady state value as breakage becomes significant and the floc size distribution approaches steady state. The shear rate does not affect the steady state D_{pf} of the flocs within experimental uncertainty.

Key Words: **fractal; floc; hydrodynamics; impeller type; steady state.**

INTRODUCTION

The removal of solid particles from a liquid suspension is often enhanced by enlarging them through shear-induced flocculation. By this process, the particles initially grow by coagulation, forming irregular floc structures within the shear field of the liquid. As the flocs grow, however, they become susceptible to breakage by fluid shear. After a certain time, the floc size distribution reaches a steady state between floc growth and breakage and it no longer changes (1, 2). Solids removal efficiency by sedimentation or filtration depends on the structure of the flocs, as this determines the relationship between floc size and density. In addition, changes in floc structure within a suspension affect macroscopic properties like viscosity (3) altering the processing requirements of cell suspensions (4–6). The porosity of flocs also determines the quality of compact parts made of ceramic particles (7). Despite its significance in numerous disciplines, the dynamic evolution of sheared floc structures has not been studied experimentally.

Most previous studies have evaluated the structure of flocs at steady state (8–10). The evolution of the floc structure is equally important, however, as it determines the steady state characteristics of the flocs and their removal efficiency. Settling velocity measurements indicate an inverse relationship between floc size and density. The reduced floc density with increasing size is usually attributed to the incorporation of fluid into the floc structure (11). These porous flocs collide with each other to form increasingly porous structures (12) until shear-induced fragmentation halts further growth of the floc size distribution. Floc structures can also be made more compact by shear-induced breakage or restructuring (13–17) as illustrated in Fig. 1. The growth, breakage, and restructuring processes govern the development of floc structures and all three occur within the complex shear field of a stirred tank.

Despite the relevance of the hydrodynamic flow field on flocculator performance, few fundamental studies of the effect of different flow fields on flocculation variables like floc size and structure have been carried out. Oldshue and Mady (18) studied the effect of impeller type and flocculator volume on particle removal at a water treatment plant using turbidity measurements. They observed different particle removal efficiencies at constant shear rate, G, for the impellers examined. Glasgow (19) compared the hydrodynamic behavior and flocculation performance of two perforated plastic paddle impeller assemblies: a 4-blade paddle and a paddle covered with cloth. The two impellers produced significantly different energy dissipation rates at the same impeller speeds, especially at low values. No significant difference between the two impellers was observed from average floc size and density measurements. McConnachie (20) evaluated three impellers (paddle, picket gate, and branched paddle) by measurements of fluid turbulent intensity, local fluid velocity, and turbidity during flocculation. He observed that each impeller produced a minimum turbidity level at a similar power input, indicating no significant difference between the performance of the three impellers. Oldshue and Trussell (21) found that the average shear rate in a stirred tank was a linear function of impeller speed, N, for the Rushton, 4-blade, and fluid foil impellers regardless of their size. How-

[1] To whom correspondence should be addressed.

0021-9797/96 $18.00

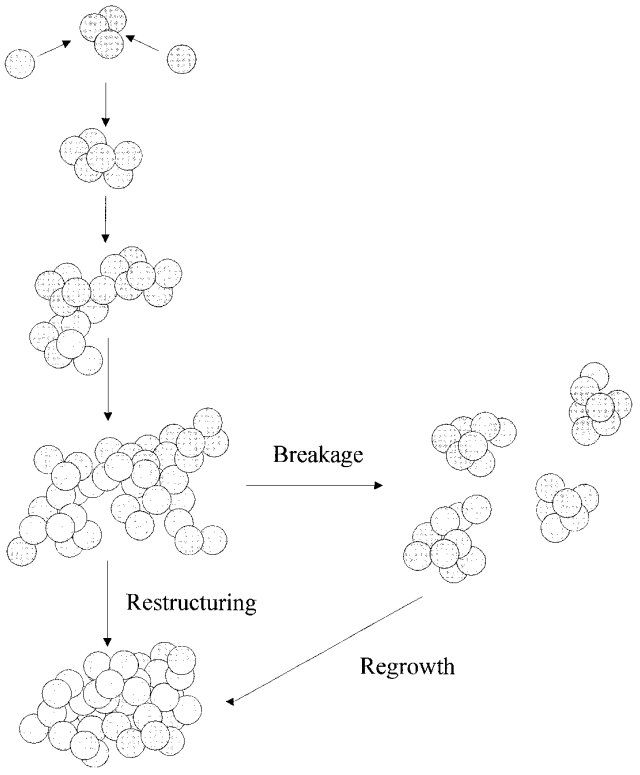

FIG. 1. Schematic of the evolution of floc structure during shear-induced flocculation.

ever, the maximum shear rate varied linearly with impeller speed for the fluid foil impeller while it varied linearly with impeller tip speed, *ND*, for the other impellers in agreement with de Boer *et al.* (22).

The objective of this study is to describe the effect of impeller type (and thus hydrodynamic flow field) on the evolution of the average floc size and structure during flocculation of polystyrene particles with aluminum sulfate in a stirred tank. The floc size and structure are monitored as a function of time using image analysis, thus characterizing the structural events leading up to the attainment of steady state.

EXPERIMENTAL

Apparatus and Procedure

Flocculation of an aqueous suspension of monodisperse, spherical, polystyrene particles (17) ($d_0 = 0.87\ \mu$m) was studied in a 2.8-liter, baffled, stirred tank (Fig. 2). The suspension was mixed using one radial flow and two axial flow impellers (Fig. 2) widely used during flocculation (21). The radial flow impeller was a high shear radial flow (Rushton) Lightnin R100 impeller. The two axial flow impellers were a 4-blade 45° pitch Lightnin A200 and a three-blade fluid foil Lightnin A310 impeller. The center of the impeller was positioned at $\frac{1}{3}$ the height of the tank (23). The solids volume fraction was $\phi = 1.4 \times 10^{-5}$, corresponding to an initial particle number concentration of 4×10^7 cm^{-3}. The flocculant was an acidic stock solution of 0.5 g/liter of aluminum sulfate hydrate ($Al_2(SO_4)_3$ $16H_2O$; Aldrich, 98%) (17). All experiments were conducted using a constant $Al_2(SO_4)_3$ $16H_2O$ concentration of 10 mg/liter, meaning that 76% of the solids mass present (88% of the solids volume) was contributed by the polystyrene particles and 24% by the precipitated $Al(OH)_3$. Sodium hydrogen carbonate ($NaHCO_3$; Aldrich, 99%) was used to buffer the suspension and the pH was kept at 7.2 ± 0.05 during all experiments (17).

The polystyrene suspension was first mixed at $G = 300$ s^{-1} for five minutes to break up any agglomerates. This procedure was checked using a control experiment in which no flocculant was added and the individual primary particles remain unflocculated under microscopic viewing. The flocculant was then added and mixed with the suspension for one minute. The impeller was then set to the desired speed.

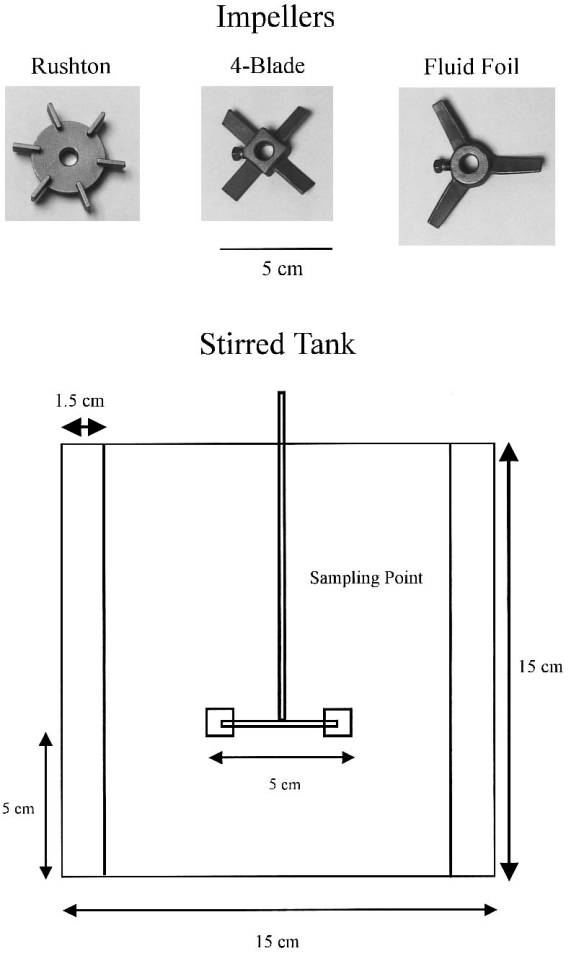

FIG. 2. Schematic diagram of the stirred tank used for the flocculation experiments and photographs of the Rushton, 4-blade, and fluid foil impellers.

Samples were removed for size analysis using the wide end of a 0.5-cm ID pipette (24). The impeller speeds were chosen to eliminate floc sedimentation and to produce floc structures unaffected by the sampling procedure. The impeller rotational velocity was measured using an optical tachometer (Onno Sokki HT-4100) and varied by less than 1 RPM.

Stirred Tank Flow Field Characterization

The turbulent shear rate within the stirred tank was characterized using the spatially averaged velocity gradient, G (25)

$$G = \left(\frac{\epsilon}{\nu}\right)^{1/2}, \qquad [1]$$

where ν is the kinematic viscosity of the suspending fluid (here, water) and ϵ is the average turbulent energy dissipation rate (17, 26)

$$\epsilon = \left(\frac{N_p N^3 D^5}{V}\right) \qquad [2]$$

where N_p is the impeller power number, N is the impeller speed, V is the stirred tank volume, and D is the impeller diameter. The N_p for the three employed impellers are (21, 23, 27): Rushton, $N_p = 5$, fluid foil, $N_p = 0.3$, and 4-blade, $N_p = 1.27$. In all experiments, the impeller Reynolds number was larger than 10^3, resulting in a relatively constant N_p for each impeller. The flow conditions within a stirred tank are heterogeneous (28), thus the averaged G in Eq. [1] does not characterize the local velocity gradients within the stirred tank or the variation in flow field produced by the various impellers (20, 29, 30). However, the use of a constant G provides a basis for comparison of the flocculation performance of the employed impellers that is consistent with previous work.

An estimate of the frequency of exposure of the flocs to the high shear impeller zone can be obtained from the circulation time, t_c (31)

$$t_c = \frac{V}{N_q N D^3}, \qquad [3]$$

where N_q is the dimensionless impeller pumping capacity: for the Rushton $N_q = 0.9$, 4-blade $N_q = 0.79$, and fluid foil $N_q = 0.56$ (23, 31). Comparison with circulation time measurements of tracer particles indicates that t_c offers a good basis for characterization of small tanks such as the one used here (21).

Floc Characterization by Image Analysis

Floc size distributions were measured using an optical microscope (Nikon Labophot) equipped with a video camera (Hitachi–Denshi). Images were digitized using a frame grabber board (DT-55, Data Translation) installed in a personal computer (DTK 486 DX4). The maximum floc length (length of a rectangle enclosing the entire floc), cross-sectional projected area, and perimeter of all the flocs in a sample was measured and recorded by image analysis software (Global Lab Image v. 2.0). These values were used to characterize the evolution of floc size (maximum length) and structure and were obtained after the viewed flocs had settled to their most stable configuration. The image analysis software identifies an area of the image as a particle if the grey values of the contiguous pixels exceed a user defined threshold value. Before analysis the software was calibrated using a slide marked at known intervals. An image of the slide was digitized and the number of pixels between two marks corresponding to a calibrated distance was recorded on the screen.

The resolution of the microscope defines the lower detection limit of the image analysis technique. Under 100× magnification the lower detection limit was 10 μm, thus the average floc sizes measured during the early stages of flocculation ($t < 1$ h) are overestimated. After the first hour of flocculation the floc structures evaluated under 100× magnification were in excellent agreement, within experimental error (± 0.05), with the results obtained at 400× magnification. This supports the assumption of a fractal-like or scale invariant floc structure (32). The floc sizes evaluated at 100× magnification were also in agreement ($\pm 7\%$) with the results obtained at 400×. The 100× magnification was therefore used in all experiments in order to sample the largest number of particles possible.

The relationship between the cross-sectional projection area, A, of a fractal-like floc and the perimeter of its projection, P, is (33):

$$A \propto P^{2/D_{pf}} \qquad [4]$$

The D_{pf} varies from $D_{pf} = 1$ for the projected area of a sphere (a circle), to $D_{pf} = 2$ for a line (e.g., a chain of particles). Li and Ganczarczyk (34) used Eq. [4] to characterize activated sludge flocs and found values of $D_{pf} = 1.13$–1.22. The value of D_{pf} is a quantitative measure of floc structure that is directly related to the surface fractal dimension, D_s, of the floc (33, 35). Image analysis of floc structure projections is a more direct and rapid measure of floc structure than light scattering and size/sedimentation velocity measurements and thus has potential for on-line application in the process industry. The mass fractal dimension of a floc, D_f, is also a measure of floc structure and varies from 1 for a line of particles to 3 for a sphere (32). Clark and Flora (17) reviewed several studies of floc structure where the D_f varied from 1.6 to 2.8. The D_{pf} derived from image analysis is a two-dimensional fractal dimension and is not directly related to D_f (36).

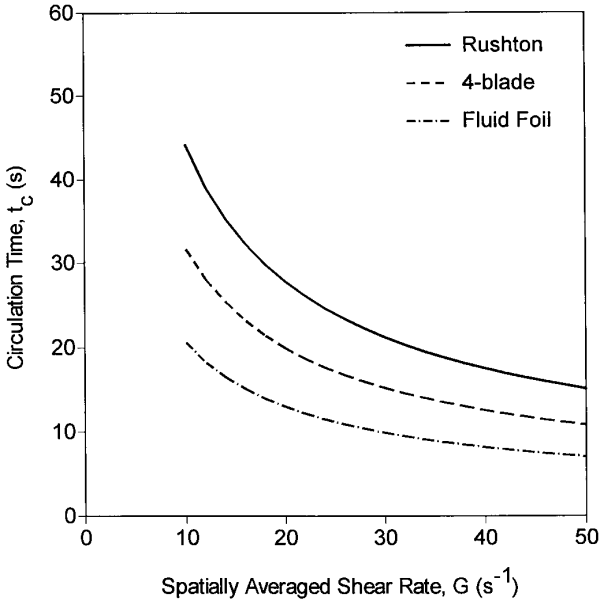

FIG. 3. Calculated circulation times, t_c, as a function of G for all three impellers.

RESULTS AND DISCUSSION

Impeller Flow Patterns and Circulation Time

First it is important to develop an understanding of the flow patterns created by the three impellers. Figure 3 shows the circulation time, t_c, of all impellers calculated as a function of G using Eq. [1–3]. For a constant G, the Rushton impeller results in the longest circulation time, followed by the 4-blade and fluid foil impellers. This is the result of the characteristic flow fields of the radial and axial flow impellers. The radial flow impeller (here, the Rushton) creates fluid flow directed radially outward from the impeller that mostly circulates into the region above the impeller. These recirculated fluid parcels then slowly return to the impeller zone by sedimentation. In contrast, the axial flow impeller produces a constant pumping action toward the bottom of the tank followed by circulation to the top and a relatively rapid return to the impeller zone (23). The short circulation time produced by the axial flow impellers increases the frequency of exposure to the high intensity shear in the impeller zone, where turbulent energy dissipation rates are much larger than in the bulk zone (37). The 4-blade impeller produces flow that is a combination of axial and radial patterns, directed downward 45° from the vertical axis (21). As a result, for a constant G, the t_c of the 4-blade is in between those of the axial and radial flow impellers.

Figure 4 shows characteristic floc pictures at various stages of flocculation using the Rushton impeller at 25 s^{-1}. After 15 min of flocculation (Fig. 4a) a bimodal floc size distribution is evident, large flocs are beginning to form but small clusters are still widespread. The largest flocs have a more irregular structure than the smaller ones as a result of the increased porosity at the larger floc sizes. After 30 min (Fig. 4b), most of the smallest clusters have been ''swept out'' and incorporated into the structure of the larger flocs, although some remain. The floc structure in Fig. 4b is clearly the result of aggregate–aggregate collisions: the floc image indicates the floc is composed of several smaller flocs packed together randomly. Visual observations at this stage of the experiment indicate that the turbidity of the suspension has dropped drastically from that of the previous sample, indicating a significant drop in the particle number concentration. The areas of the flocs that are not in focus are regions that extend upward toward the microscope eyepiece, preventing clear resolution of the entire floc. After 1 h (Fig. 4c), the average floc structure has become larger and even more irregular as the flocs continue to grow by aggregate–aggregate collisions. After 1 h the flocs observed visually have roughly the same maximum length, indicating that the floc size distribution has narrowed considerably from its early bimodal stages (Fig. 4a). Finally, after 1.5 h (Fig. 4d), the flocs have grown slightly larger but are not significantly larger or more irregular than the floc in Fig. 4c. Subsequent samples show no significant difference in size or structure.

Figure 5 shows the evolution of the number average maximum floc length, L_n, at (a) $G = 15$, (b) 25, and (c) 50 s^{-1} for all impellers. All results represent the average of at least two replicate experiments, error bars indicate reproducibility unless stated otherwise. Initially, floc growth is dominant so L_n rapidly increases. As the flocs become larger, shear-induced fragmentation becomes significant and competes with coagulation, slowing down the rate of floc growth. Eventually, a steady state is reached between shear-induced coagulation and fragmentation and L_n no longer changes (2). Figure 5a shows that a steady state floc size is reached first by the axial impellers, followed by the Rushton.

The type of impeller affects the hydrodynamic environment experienced by the flocs and therefore determines the kinetics of floc growth and breakage by shear. At 15 s^{-1}, the largest flocs are produced by the Rushton impeller (Fig. 5a). Although the radial flow impeller creates considerable shear (21), the frequency of circulation through the high shear impeller zone is lower than that for the other two impellers (Fig. 3). The 4-blade and fluid foil impellers pump fluid downward resulting in a more rapid recirculation of flocs through the impeller zone than the Rushton impeller. In contrast, the Rushton impeller results in a relatively higher residence time for the flocs in the more gentle upper bulk zone than the other two impellers. As a result, it takes longer for the floc size to reach steady state with the radial than with the axial flow impellers. Also, the Rushton impeller produces the largest flocs at steady state. Steady state is attained faster at 25 s^{-1} than at 15 s^{-1} because of the accelerated coagulation and fragmentation, in agreement with Reich

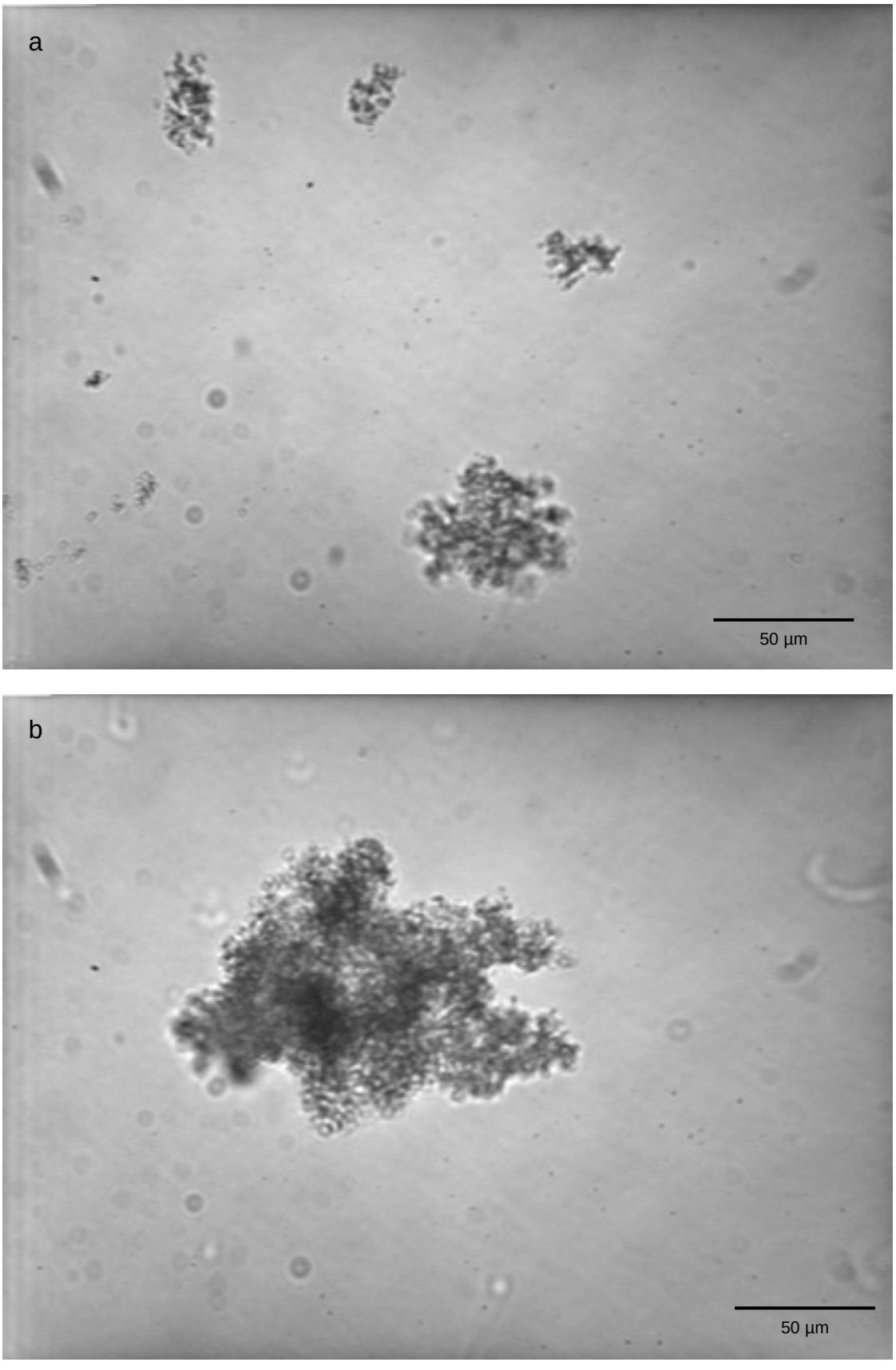

FIG. 4. Micrographs of flocs formed using the Rushton impeller at 15 s^{-1} after (a) 15 (b) 30 (c) 60 and (d) 90 min. A bimodal size distribution is produced initially, large irregular flocs and small compact ones coexist. Later on, aggregate–aggregate collisions produce larger, more irregular flocs until steady state is reached.

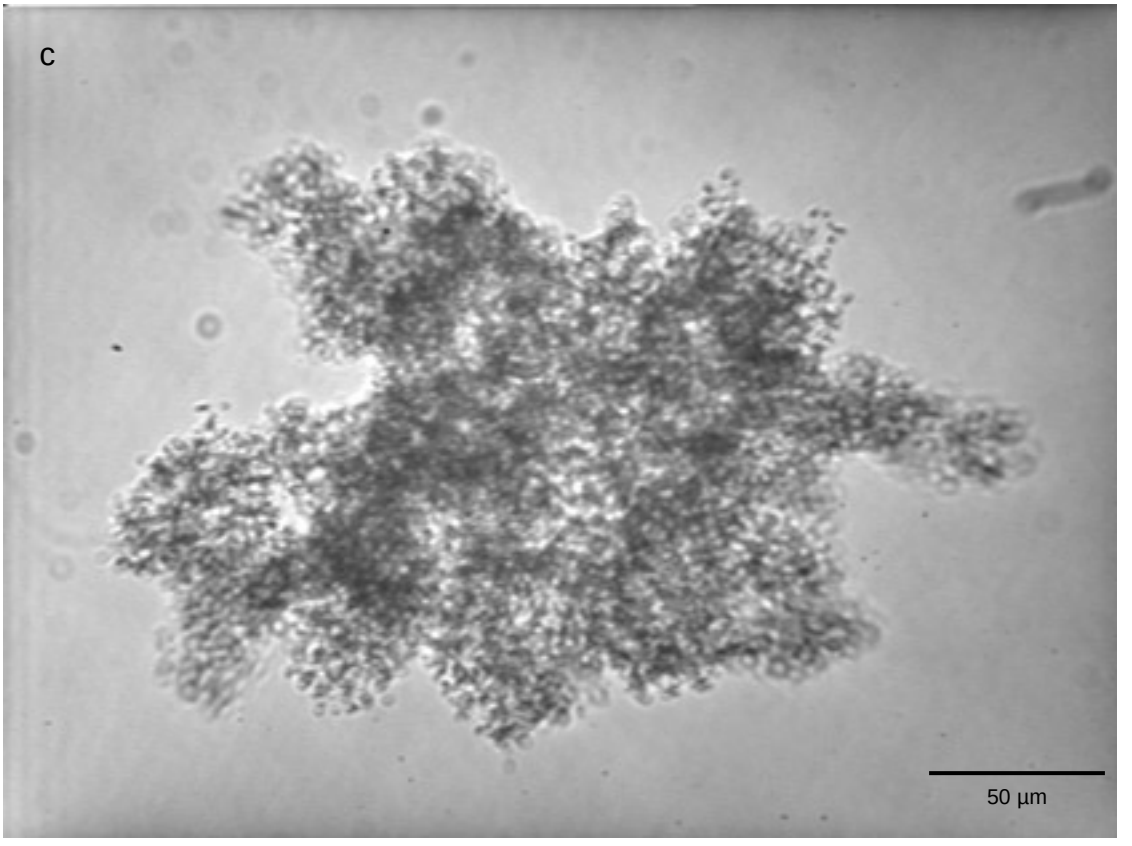
c
50 µm

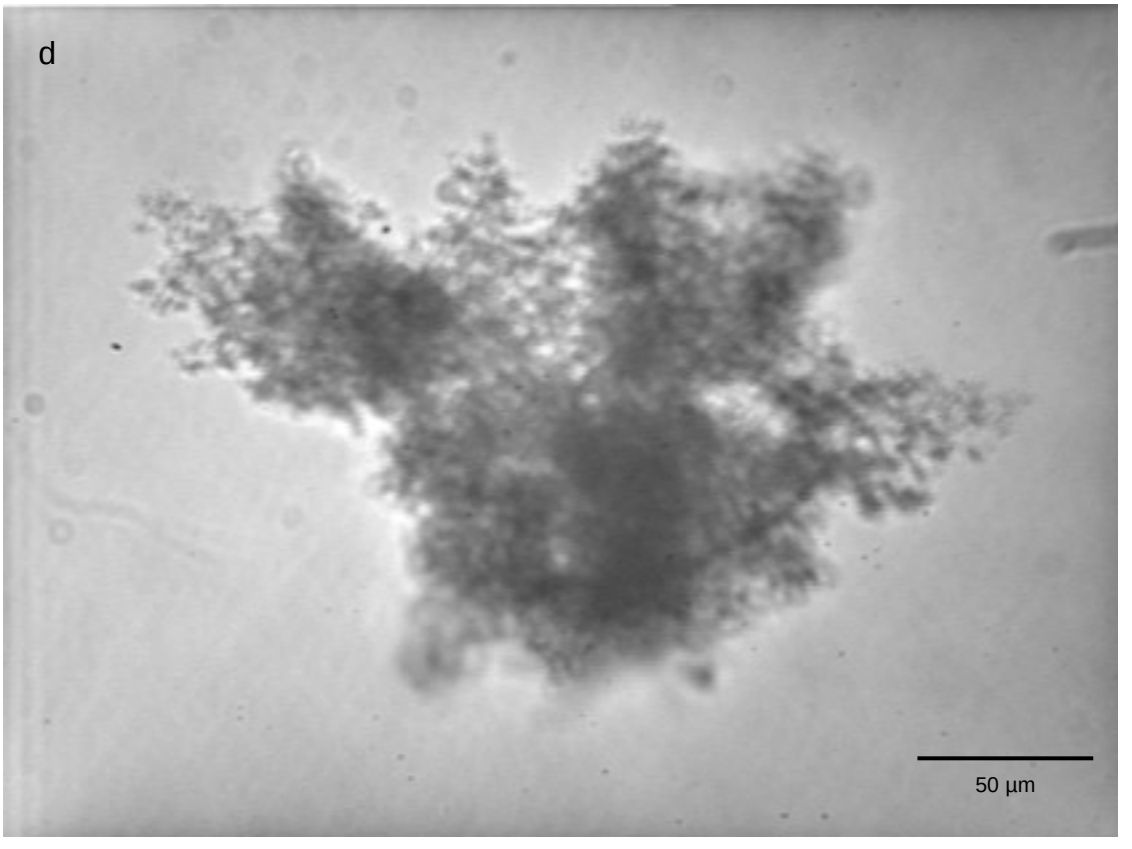
d
50 µm

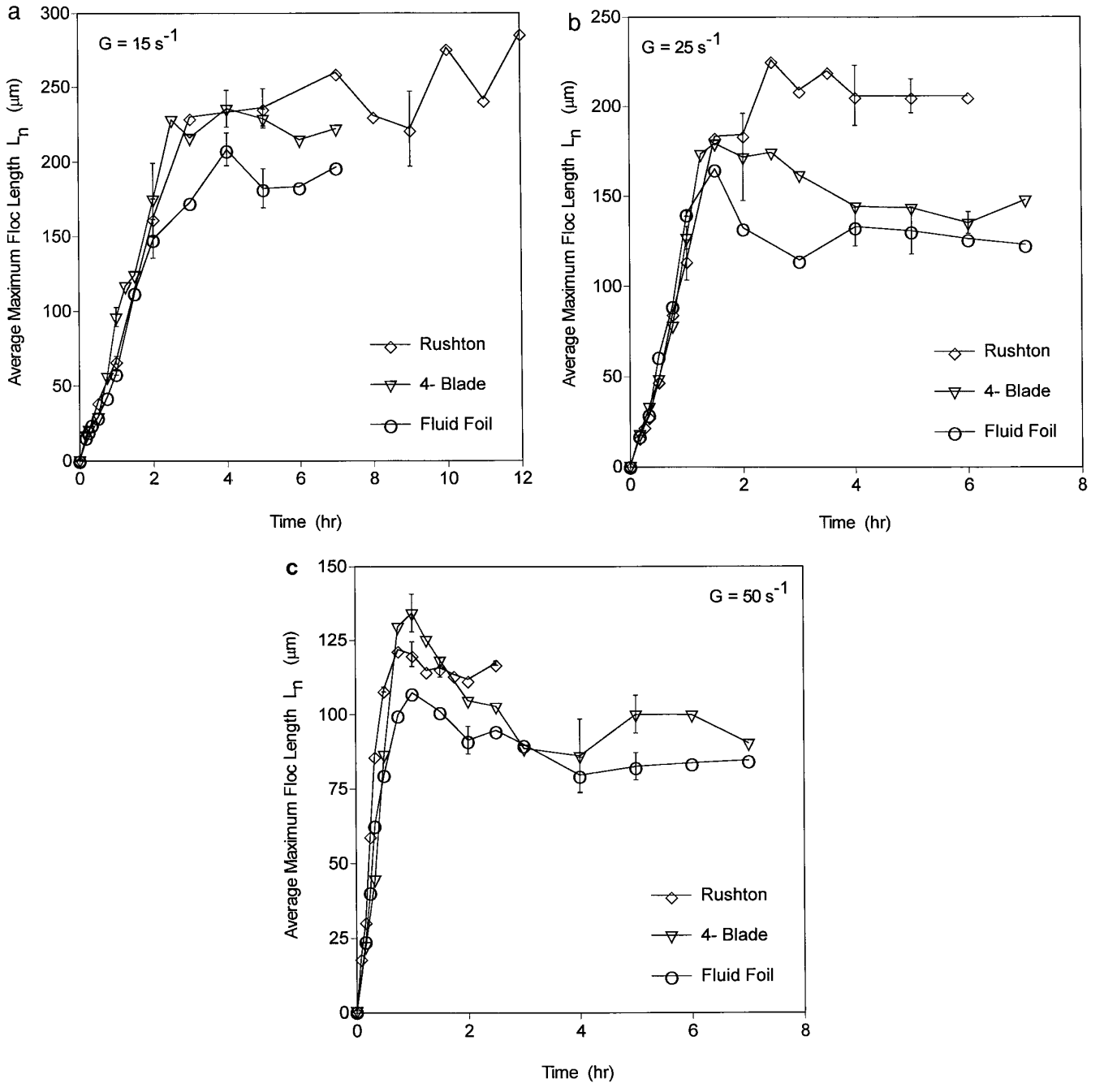

FIG. 5. The evolution of the average maximum floc length, L_n, for all three impellers at (a) $G = 15$, (b) 25, and (c) 50 s^{-1}. The L_n increases rapidly during the growth-dominated regime and levels off as floc breakage becomes significant. The Rushton impeller produces the largest flocs but at the lowest rate. A maximum in L_n is observed at 50 s^{-1} for the 4-blade and fluid foil impellers.

and Vold and others (2, 38, 39). Increased shear rates produce a significant decrease in the steady state floc length as a result of the increased fragmentation (Fig. 5b). The effect of impeller type is compressed somewhat by the higher impeller speed.

At $G = 50$ s^{-1}, L_n reaches a maximum before decreasing to its steady state value for both axial flow impellers (Fig. 5c). This effect is likely the result of restructuring by the more intense shear forces at this shear rate. More specifically, the compaction resulting from the more frequent exposure of the flocs to the impeller zone decreases the L_n. The increased mixing and circulation at higher shear rates leads to increased exposure of the flocs to the impeller zone and thus increased likelihood of floc restructuring by shear forces. Floc restructuring is more pronounced for the axial flow impellers because these flocs have experienced the high

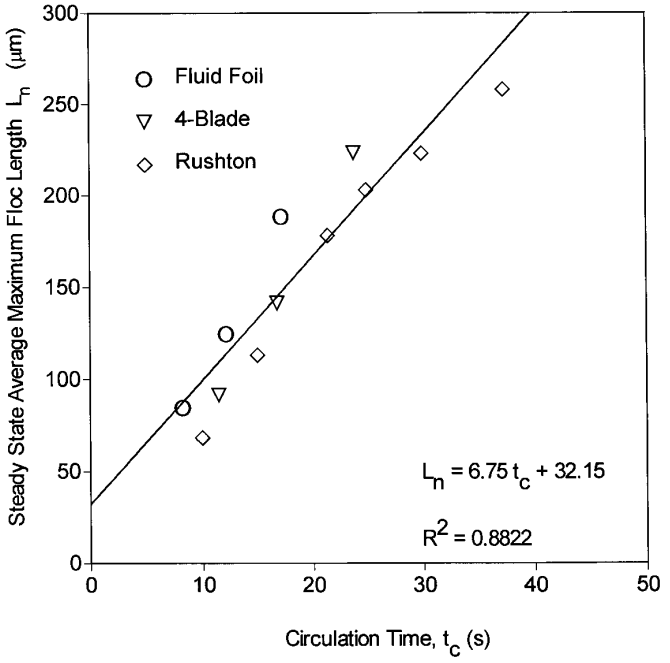

FIG. 6. The steady state average maximum floc length, L_n, as a function of the circulation time, t_c. At a constant t_c, the fluid foil produces the largest flocs, followed by the 4-blade and Rushton as a result of the direction of the fluid velocity at the impeller.

shear impeller zone more frequently than with the Rushton impeller.

Figure 5 showed that at a constant G, different impellers produce different floc sizes at steady state. One possible explanation is that all significant floc breakage occurs within the region of highest shear: the impeller zone. This reduces the description of floc breakage to a characterization of the impeller zone and the rate of exchange between the impeller zone and the relatively quiescent bulk region outside of it (6, 40). This model of floc breakage assumes the flocs are only broken upon exposure to the impeller stream. While breakage of flocs with very open structures is possible in the bulk zone of a stirred tank (40), the relatively compact structures produced during these experiments (Fig. 4) can be resistant to this mode of breakage.

While most previous studies have correlated floc size with the average shear rate (characteristic of the bulk region), an objective of this work is to evaluate the use of the impeller tip speed, *ND* (characteristic velocity of the impeller zone) and the circulation time, t_c (characteristic of the inverse frequency of exposure to the impeller zone and thus breakage frequency) for correlation with the average floc size, L_n, at steady state. Figure 6 shows the steady state L_n as a function of t_c for all impellers. In Fig. 6, the L_n increases linearly with circulation time as a result of the decreased floc breakage frequency. However, at a constant circulation time, the fluid foil produces the largest flocs, followed by the 4-blade and the Rushton. This may result from the characteristics of the velocity gradient at the impeller. In Fig. 6, as the flow progresses from purely axial flow (fluid foil), to the intermediate case (4-blade), to radial flow (Rushton), smaller flocs are produced at a constant circulation time. As the flocs approach the impeller zone during circulation, the least intense shearing will be experienced by flocs that do not change direction rapidly as they approach and pass the impeller. This behavior is expected for flocs circulating through the impeller zone of the fluid foil: flocs are circulated axially downward through the impeller zone and return to the top of the tank by recirculation at the tank bottom. In contrast, the Rushton impeller produces flow perpendicular to the original direction of the approaching flocs, producing a more abrupt shearing because of its distinct velocity gradient. The 4-blade impeller produces a flow that is a combination of that of the fluid foil and Rushton, thus the floc size result is intermediate as well. It is clear that complete characterization of floc breakage frequency in the impeller zone requires knowledge not only of the frequency of floc exposure to the impeller zone but also of the characteristic velocity gradient in the impeller zone.

The speed of the impeller tip, *ND*, is indicative of the impeller zone velocity gradient (21). Figure 7 shows the effect of impeller tip speed on the steady state floc size for all three impellers. For all impellers, increasing the impeller tip speed decreases the steady state average max-

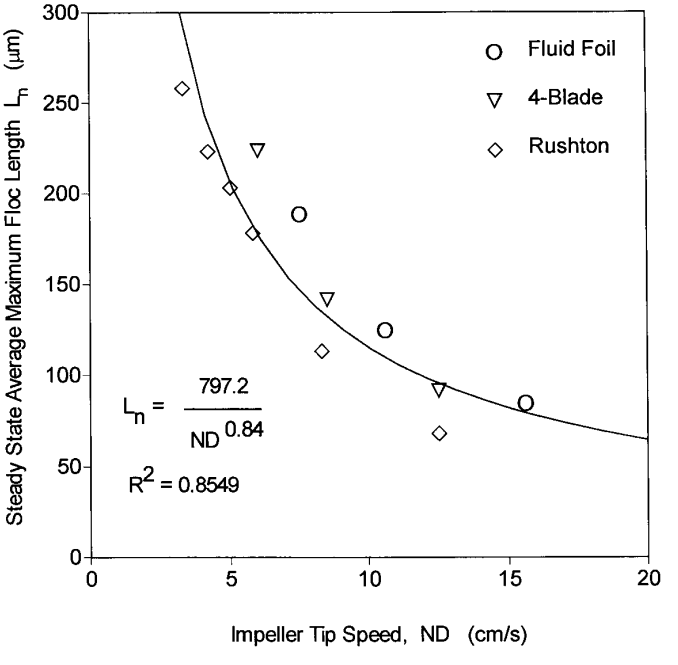

FIG. 7. The steady state average maximum floc length, L_n, as a function of the impeller tip speed, *ND*. At a constant *ND*, the fluid foil produces the largest flocs, followed by the 4-blade and Rushton impellers.

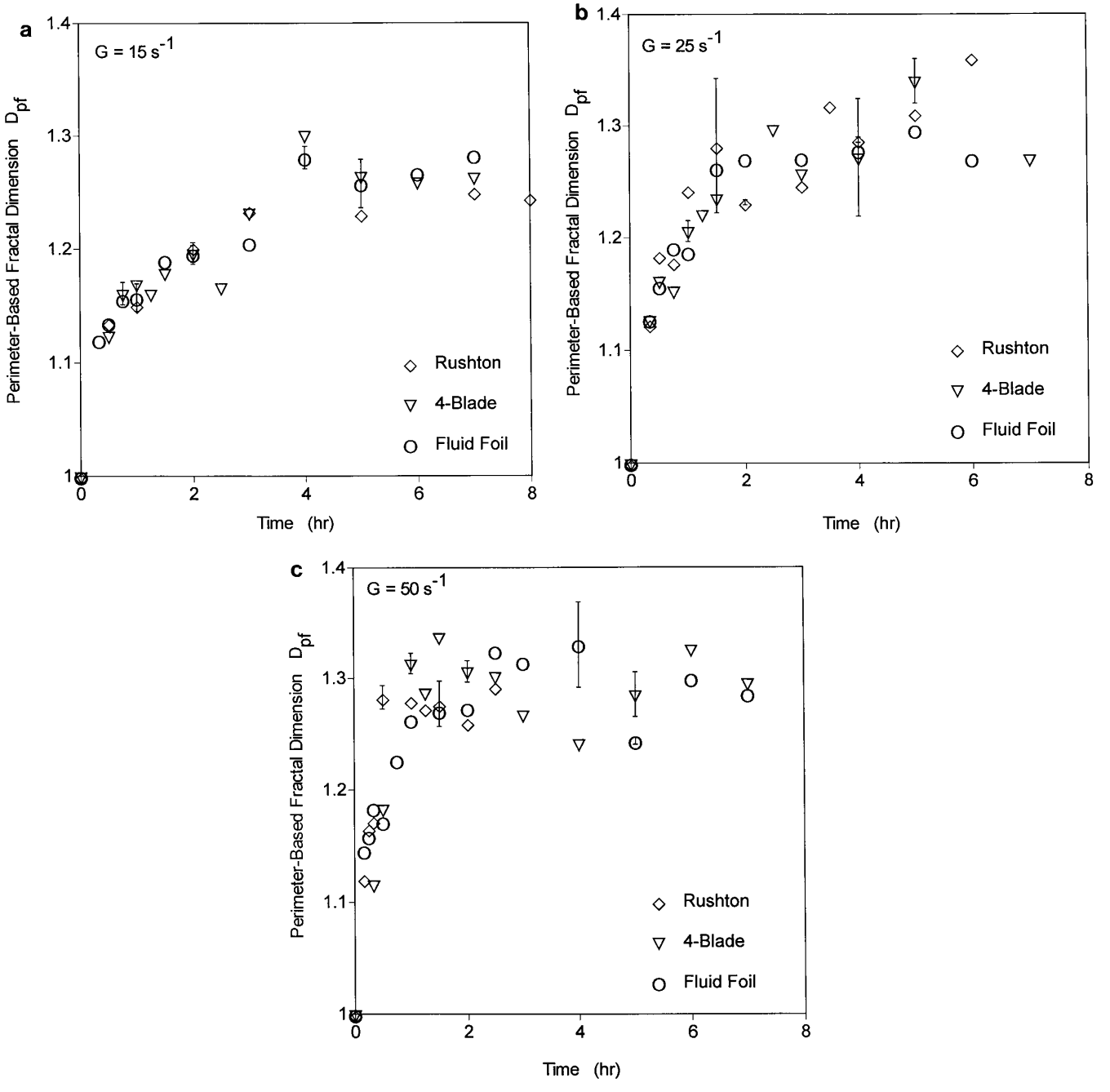

FIG. 8. The time evolution of the perimeter-based fractal dimension, D_{pf}, for the three impellers at (a) $G = 15$, (b) 25, and (c) 50 s^{-1}. An asymptotic value of D_{pf} is reached as fragmentation becomes significant. All three impellers produce the same evolutionary behavior but increased shear rates accelerate steady state attainment. Restructuring by the increased shear stresses produces a maximum in the D_{pf} prior to steady state at $G = 50$ s^{-1} for the axial flow impellers.

imum floc length. The data are best correlated by a power law function, similar to the relationships found between floc size and the average shear rate, G (8). It should be noted, however, that a power law fit of the steady state L_n as a function of G yielded a weaker correlation ($R^2 = 0.796$) than for t_c ($R^2 = 0.882$) or ND ($R^2 = 0.855$). At a constant tip speed, the same trend observed in Fig. 6 is seen in Fig. 7: the largest flocs are produced by the fluid foil, followed by the 4-blade and the Rushton. This may also result from the different direction of the velocity gradient at the impeller with changing impeller types. The results in Figs. 6 and 7 indicate that the frequency

of exposure to the impeller zone and the zone's characteristic velocity gradient are important design parameters for minimizing floc breakage and thus maximizing floc size.

Effect of Impeller Type and Shear Rate on the Evolution of Floc Structure

Figure 8 shows the evolution of the perimeter-based fractal dimension for (a) $G = 15$, (b) 25 and (c) 50 s^{-1} for the three impellers. Initially the D_{pf} increases, indicating that more open floc structures are formed as floc growth dominates, regardless of the impeller type. Later on, D_{pf} reaches steady state as fragmentation becomes significant and impedes the production of more irregular structures. The impeller type does not appear to influence the evolution of the D_{pf}, since the data in Fig. 8a closely follow the same evolution pattern. More scatter in D_{pf} is observed at $G = 25$ s^{-1} (Fig. 8b) than at $G = 15$ s^{-1} (Fig. 8a), although this decreases as steady state is approached and the distribution of floc structures narrows (39). For all impellers, the evolution of D_{pf} collapses onto one curve at a constant shear rate. A slightly higher steady state value of D_{pf} is reached at 25 s^{-1} than at 15 s^{-1}, although this may not be significant within the uncertainty of the D_{pf} determination.

At $G = 50$ s^{-1}, the D_{pf} of the flocs increases rapidly at early times, indicating the formation of open flocs while shear-induced growth dominates (Fig. 8c). From then on, significant floc breakage takes place, making the floc structure more compact (decreasing D_{pf}) as a steady state is attained with respect to floc size and structure. This is more significant for the two axial flow impellers: in Fig. 8c the D_{pf} produced by these impellers gradually decreases to its steady state value. This is consistent with the maximum in L_n observed in Fig. 5c at $t = 1$ h for the axial flow impellers. Thus, it is possible that the more open floc structures (larger D_{pf}) increase the floc collision rates and subsequently their growth resulting in larger particles (larger L_n). Later on, however, these rather weak flocs break by shear-induced fragmentation and reach a steady state as with the lower shear rates.

CONCLUSIONS

The evolution of the polystyrene–alum floc structures produced by various impellers and spatially averaged velocity gradients, G, has been investigated. The average floc length, L_n, increased rapidly during floc growth and leveled off at a steady state value that increased with decreasing G with all impellers. The Rushton impeller produced the largest flocs, followed by the 4-blade and the fluid foil impellers at all G values. The Rushton impeller results in the largest circulation time and thus the lowest frequency of exposure to the impeller zone in the stirred tank. However, at a constant circulation time and impeller tip speed, the fluid foil impeller produced the largest flocs, followed by the 4-blade and the Rushton impellers. This is attributed to the greater shearing action of the radial than the axial impeller in the impeller zone.

The two-dimensional fractal dimension of the flocs, D_{pf}, was used to quantify their structure. The D_{pf} of flocs produced by all three impellers increased rapidly during the early (growth-dominated) stage of flocculation. The evolution of D_{pf} was not influenced by impeller type at $G = 15$ and 25 s^{-1}. At $G = 50$ s^{-1}, a maximum in D_{pf} is observed prior to attainment of steady state for the two axial flow impellers as a result of the increased floc exposure at the impeller zone. The G does not affect the steady state D_{pf} value of the flocs at constant flocculant concentration within experimental uncertainty.

ACKNOWLEDGMENTS

Support by the National Science Foundation, Grant CTS-8957042, Genencor International B. V., and a graduate fellowship from the Quantum Chemical Corporation are gratefully acknowledged.

REFERENCES

1. Blatz, P. J., and Tobolsky, A. V., *J. Phys. Chem.* **49,** 77 (1945).
2. Reich, I., and R. D. Vold, *J. Phys. Chem.* **63,** 1497 (1959).
3. Gillespie, T., *J. Colloid Interface Sci.* **94,** 166 (1983).
4. Roels, J. A., Van den Berg, J., and Voncken, R. M., *Biotech. Bioeng.* **31,** 19 (1988).
5. Cooke, M., *in* ''Processing of Solid-Liquid Suspensions'' (P. A. Shamlou, Ed.), p. 192. Butterworth Heinemann, Oxford, 1993.
6. Shamlou, P. A., and Tichener-Hooker, N., *in* ''Processing of Solid-Liquid Suspensions'' (P. A. Shamlou, Ed.), p. 1. Butterworth Heinemann, Oxford, 1993.
7. Pierre, A. C., Ma, K., and Barker, C., *J. Mater. Sci.* **30,** 2176 (1995).
8. Tambo, N., and Watanabe, Y., *Water Res.* **13,** 429 (1979).
9. Klimpel, R. C., and R. Hogg, *J. Colloid Interface Sci.* **113,** 121 (1986).
10. Logan, B. E., and Kilps, J. R., *Water Res.* **21,** 443 (1995).
11. Tambo, N., *Water Supply* **9,** 1 (1991).
12. Francois, R. J., and Van Haute, A. A., *in* ''Chemistry for the Protection of the Environment'' (L. Pawlowski, Ed.). Elsevier, Amsterdam, 1984.
13. Thomas, D. G., *AIChE J.* **10,** 517 (1964).
14. Sonntag, R. C., and Russel, W. B., *J. Colloid Interface Sci.* **113,** 399 (1986).
15. Francois, R. J., *Water Res.* **21,** 523 (1987).
16. Jullien, R., and Meakin, P., *J. Colloid Interface Sci.* **127,** 265 (1989).
17. Clark, M. M., and Flora, J. R. V., *J. Colloid Interface Sci.* **147,** 407 (1991).
18. Oldshue, J. Y., and Mady, O. B., *Chem. Eng. Prog.* **74,** 103 (1978).
19. Glasgow, L. A., *Chem. Eng. Commun.* **98,** 155 (1990).
20. McConnachie, G. L., *J. Env. Eng.* **117,** 731 (1991).
21. Oldshue, J. Y., and Trussell, R. R., *in* ''Mixing in Coagulation and Flocculation'' (A. Amirtharajah and M. Clark, Eds.). American Water Works Research Foundation, Denver, 1991.
22. de Boer, G. B. J., Hoedemakers, G. F. M., and Thoenes, D., *Chem. Eng. Res. Des.* **67,** 301 (1989).
23. Holland, F. A., and Chapman, F. S., ''Liquid Mixing and Processing in Stirred Tanks,'' p. 78. Reinhold, New York, 1966.
24. Gibbs, R. J., and Konwar, L. N., *Env. Sci. Tech.* **16,** 119 (1982).

25. Camp, T. R., and Stein, P. G., *J. Boston Soc. Civ. Eng.* **30,** 219 (1943).
26. Godfrey, J. C., Obi, F. I. N., and Reeve, R. N., *Chem. Eng. Prog.* **85,** 61 (1989).
27. Shaw, J. A., *Chem. Eng. Prog.* **90,** 45 (1994).
28. Cutter, L. A., *AIChE J.* **12,** 35 (1966).
29. Cleasby, J. L., *J. Env. Eng.* **110,** 875 (1984).
30. Clark, M. M., *J. Env. Eng.* **111,** 741 (1985).
31. Oldshue, J. Y., ''Fluid Mixing Technology.'' McGraw–Hill, New York, 1984.
32. Mandelbrot, B. B., ''The Fractal Geometry of Nature.'' Freeman, New York, 1987.
33. Mandelbrot, B. B., Passoja, D. E., and Paullay, A. J., *Nature* **308,** 721 (1984).
34. Li, D., and Ganczarczyk, J. J., *Env. Sci. Tech.* **23,** 1385 (1989).
35. Schroeder, M., ''Fractals, Chaos, Power Laws.'' Freeman, New York, 1991.
36. Meakin, P., *Adv. Colloid Interface Sci.* **28,** 249 (1988).
37. Kim, Y. H., and Glasgow, L. A., *Ind. Eng. Chem. Res.* **26,** 1604 (1987).
38. Oles, V., *J. Colloid Interface Sci.* **154,** 351 (1992).
39. Spicer, P. T., and Pratsinis, S. E., *Wat. Res.* **30,** 1049 (1996).
40. Kusters, K. A., ''The Influence of Turbulence on Aggregation of Small Particles in Agitated Vessels,'' Ph.D. thesis, Eindhoven University of Technology, The Netherlands, 1991.